Rapid production of large-area deep sub-wavelength hybrid structures by femtosecond laser light-field tailoring

Lei Wang,[1] Qi-Dai Chen,[1,a)] Rui Yang,[1] Bin-Bin Xu,[1] Hai-Yu Wang,[1] Hai Yang,[2] Cheng-Song Huo,[2] Hong-Bo Sun,[1,3,a)] and Hai-Ling Tu[2]
[1]*State Key Laboratory on Integrated Optoelectronics, College of Electronic Science and Engineering, Jilin University, 2699 Qianjin Street, Changchun 130012, China*
[2]*General Research Institute for Nonferrous Metals, Beijing 100088, China*
[3]*College of Physics, Jilin University, 119 Jiefang Road, Changchun 130023, China*

(Received 13 October 2013; accepted 7 November 2013; published online 21 January 2014)

The goal of creation of large-area deep sub-wavelength nanostructures by femtosecond laser irradiation onto various materials is being hindered by the limited coherence length. Here, we report solution of the problem by light field tailoring of the incident beam with a phase mask, which serves generation of wavelets. Direct interference between the wavelets, here the first-order diffracted beams, and interference between a wavelet and its induced waves such as surface plasmon polariton are responsible for creation of micrograting and superimposed nanogratings, respectively. The principle of wavelets interference enables extension of uniformly induced hybrid structures containing deep sub-wavelength nanofeatures to macro-dimension. © *2014 AIP Publishing LLC*. [http://dx.doi.org/10.1063/1.4832878]

It is well-known that periodic micro-nanostructures can be induced by a single laser beam onto the surface of various materials such as metals, semiconductors, and transparent media.[1–3] The structure periods are generally of the order of half the laser wavelength for continuous or nanosecond pulsed laser irradiation as a result of interference between the incident and scattered light.[4] Furthermore, deep sub-wavelength structures with period less than $\lambda/3$ are achievable when femtosecond pulsed lasers are adopted.[5] This is attributed to interactions between the incident laser and the induced surface waves such as SPP (surface plasmon polariton) and SHG (second-harmonic generation).[6–8] The production of deep-subwavelength structures is attracting significant research focus since it may provide an avenue towards nanophotonic components and devices.[9–13] However, a major obstacle toward this goal is the limit coherence length of femtosecond lasers, typically, 30 μm for a 100 fs, 800 nm wavelength beam.[9,14] Consequently, deep-subwavelength gratings are usually only observed at the bottom of ablative pits and are limited to dimensions of only a few tens of micrometers.[1–8,15–17] For the purpose of rapid fabrication of large-area deep subwavelength nanostructures, here we report an approach using a phase mask to convert the incident light field into periodic array of wavelets. Direct interference ablation[18,19] by the neighboring wavelets, aided by a lateral mask scanning, leads to large-area uniform nanogratings that were spaced by micro-columns, i.e., hierarchical structures composing of sub-wavelength features.

Fig. 1(a) shows the schematic illustration of the femtosecond laser wavelet interference ablation system, for which near infrared femtosecond laser pulses were attained using a Ti:sapphire regenerative amplifier laser system (Spectra Physics) operating at a wavelength of 800 nm as usually utilized.[20,21] The laser had a pulse duration of 100 femtoseconds and had a tunable repetition rate ranging from 1 to 1000 Hz. The beam was focused using a cylindrical lens, with a focal length $f = 110$ mm, through a silica zero-order-nulled phase mask with a period $\Lambda = 3.33$ μm onto the substrate. The beam was compressed by the cylindrical lens into a rectangular shape of 1 cm in length and about 2–10 μm in width, and was diffracted into +1 order and −1 order. The space between the phase mask and focus of the rectangular beam was about 3–5 mm. The substrate was scanned at a optimized speed by a step motor controlled by computer, which makes it possible to fabricate large-area structures. The sample we utilized here is polycrystal ZnS (Zinc Sulfide, 3 mm thick, with surface roughness less than 100 nm), from which typical structured surfaces with rainbow colors are shown in Fig. 1(b). It took less than 100 s to complete scanning of the 5 mm × 5 mm area, and the pattern is found consisting of micro-nano hierarchical structures as exhibited later in Fig. 3.

The rainbow patterns were produced by single femtosecond laser beam scanning, and its formation mechanism may be understood as follows. In the progress of femtosecond laser interaction with materials, a widely accepted scenario

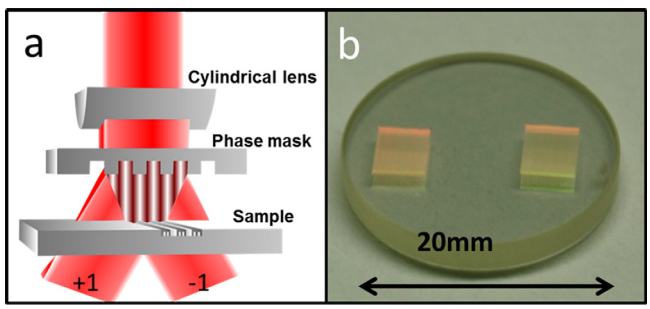

FIG. 1. Production of large-area hierarchical structure composed of deep-subwavelength nanogratings. (a) Schematic of femtosecond laser interference ablation through light field tailoring by a cylindrical lens and phase mask interference. (b) Photography of a sample fabricated by femtosecond laser interference ablation.

[a)]Authors to whom correspondence should be addressed. Electronic addresses: chenqd@jlu.edu.cn and hbsun@jlu.edu.cn

 © 2014 AIP Publishing LLC

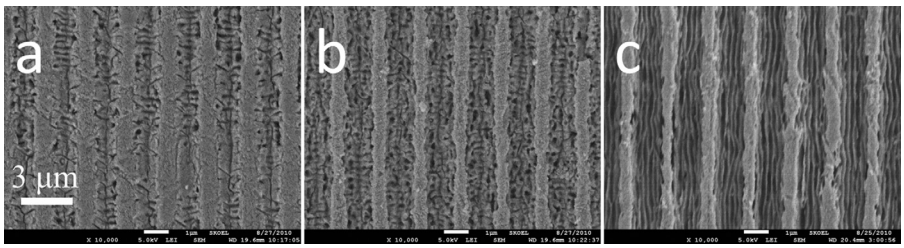

FIG. 2. Scanning electron micrograph of nanostructures with different laser repetition rates when the laser focus was scanned relative to the mask grating direction. (50 μm/s, vertical direction in this figure, and laser pulse energy of 1 mJ/cm^2). (a) 10 Hz, (b) 20 Hz, and (c) 50 Hz.

for origination of periodic structures is the interference between the incident femtosecond laser beam with the excited surface waves. Regardless of SPP or SHG induced by femtosecond laser,[6–8] which is still controversial, it has been experimentally observed that the laser power, repetition rate, incident angle, and beam polarization are playing key roles in determining the morphologies of the induced structures. The time scale of laser photon absorption by electrons in materials, set by the laser pulse width, is several tens of femtoseconds. Surface waves were launched in the meantime. Within this timeframe, photons in the excitation intensity maximum of the wavelet interference fringes are preferentially absorbed by electrons via multiphoton absorption mechanism,[22] and then an avalanche of electron excitation occurs due to a linear photon absorption by the seeded electrons.[23] With an appropriate light intensity chosen, the ultimate matter pattern as shown in Figs. 1(b) and 3 should be a faithful reflection of the transient light pattern of the interference.

In the hierarchical structures, the first-level gratings were reasonably attributed to the first order diffraction of the phase mask. There is no particular reason to choose the current parameters since the same interference principle is applicable to mask of different periods only if it is larger than $\lambda/2$. However, large-period mask helps to increase the area of nanograting region, which is important for nano-feature dominated applications. The nanostructures, located inside the light intensity maximum fringe where material is preferentially ablated, should be resulted from the interference of the diffracted wavelets and the induced waves. It is interesting to notice that deep-subwavelength structures are not possibly fabricated by a single shot laser pulse ablation, but sequential exposures by more than one shot is critical. This implies the vital role played by the seed structures produced in the initial shot of irradiation, which tailor the ensuing light field. SEM (scanning electron microscopic, JEOL JSM-6700F) images (Fig. 2) demonstrate the evolution of subwavelength nanostructures with accumulation of laser pulses. For the current case, the scanning speed is 50 μm/s parallel to the 1.67 μm micrograting direction, and the focal point is 10 μm wide. When the repetition rate is set to 10 Hz, there's neither periodic structure nor polarization-dependent ablation trace [Fig. 2(a)]. When the repetition rate increases to 20 Hz, nanostructures appear and they are randomly distributed in the ablated area [Fig. 2(b)]. Periodicity of nanostructures becomes visible at 50 Hz repetition rate [Fig. 2(c)]. The nanogratings superimposed on the microgratings lead to hiearchical structures. Here, incident laser energy is kept at 1 mJ/cm^2.

The period of nanogratings is around 210 nm, which changes a little with the laser pulse energy. In this course, the duty ratio of nanograting area in one cycle is more apparently tuned (Fig. 3). For a typical low power, i.e., 0.16 mJ/cm^2 measured before cylindrical lens, near the ablation threshold, width of nanograting area is about 0.3 of the entire micrograting region of period of 1.67 μm. When the power reaches 0.3 mJ/cm^2, the ratio increases to 0.7. When the power is tuned to as high as 1 mJ/cm^2, the ratio is higher than 0.9, meaning that nanogratings extend to almost the entire laser-irradiated area.

Not only the nanograting duty ratio in the hierarchical structures but also the orientation of nanogratings relative to the micrograting is freely adjustable by choosing different incident beam polarizations. The nanogratings fabricated under pulse energy of 0.2 mJ/cm^2 and scanning speed of 100 μm/s are parallel, 45°-tilt, and perpendicular to the microgratings (Fig. 4). It should be mentioned that the nature of the induced wave is not investigated deeply in the current research since it is still a long-term-debate hot topic in ultrafast laser-matter interaction physics.[1,6,24–27] However, the straightforward polarization dependent nanograting orientations on the laser pulse energy tend to support the SPP model. Localized SPP modes may be launched upon generation of free electrons as a result of the strong femtosecond laser irradiation. The SPP mode in the seed nanostructures responds to external light-field excitation following its polarization.

Period of about 210 nm can be explained by the Drude-like mode. Dielectric constant ε^* of the plasma is determined by the largely occupied valence bands ($n_0 = 1 \times 10^{23}$ cm^{-3}) and the free-carrier response of excited electrons,[28,29]

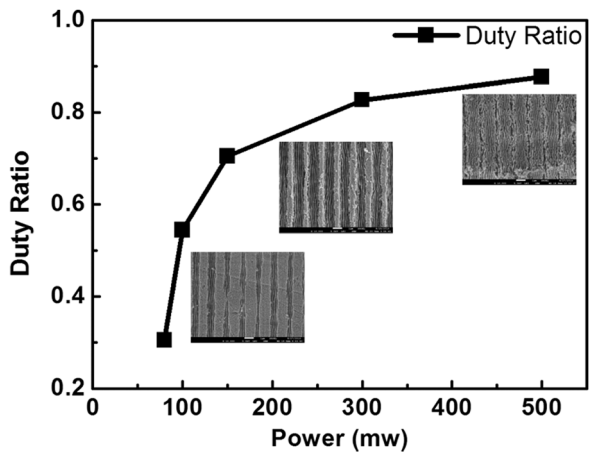

FIG. 3. Duty ratio of nanograting area in the entire micrograting region versus the pulse energy. The repetition rate is 1000 Hz.

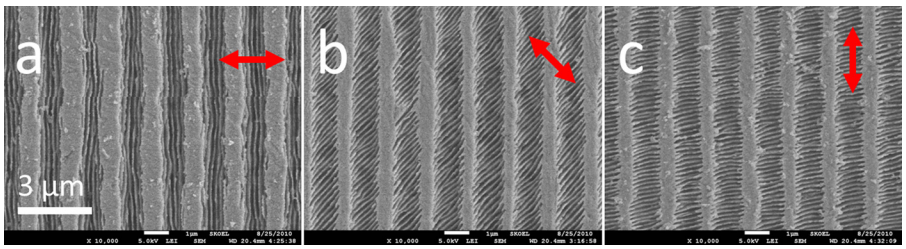

FIG. 4. Nanograting orientation tuning by changing the incident laser beam polarization. The red arrows represent different laser field polarized at (a) perpendicular, (b) 45° tilted, and (c) parallel to the micrograting direction. All the structures are fabricated under laser pulse energy of 0.2 mJ/cm^2, and scanning speed of 100 μm/s.

$$\varepsilon* = 1 + (\varepsilon_{\mathrm{ZnS}} - 1)\left(1 - \frac{n_{eh}}{n_0}\right) - \frac{w_p^2}{w^2}\frac{1}{1 + i(w\tau_D)^{-1}} = \varepsilon_1 + i\varepsilon_2, \tag{1}$$

$$\text{where,} \quad \mathrm{w} = \frac{2\pi \mathrm{c}}{\lambda}, \quad w_p^2 = \frac{n_{eh}e^2}{\varepsilon_0 m_{opt} m_e}. \tag{2}$$

Considering the environment is air, the effective dielectric constant ε is

$$\frac{1}{\varepsilon} = \frac{1}{\varepsilon*} + \frac{1}{\varepsilon_s}, \quad \text{also n} = \sqrt{\varepsilon}. \tag{3}$$

Period of SPP is defined as

$$\Lambda_{sp} = \frac{2\pi}{k_{sp}}, \quad \text{while} \quad K_{sp} = \frac{\mathrm{w}}{c/\mathrm{n}} = k_{\mathrm{sp}} + iI_{\mathrm{sp}}. \tag{4}$$

Period of structures Λ is half of SPP for the same effect of the massive excitation of electrons and the corresponding holes just as equation.

$$\Lambda = \Lambda_{sp}/2. \tag{5}$$

Curve of structure period dependence on excited electrons density was plotted in Fig. 5. As the power of light increases, electrons are excited especially strong in the position (a) when the real part of dielectric constant is 0. Then the electrons are modulated to form SPP propagating along the polarization of light. When the power is increased to ensure that n_{eh} is more than $1 \times 10^{22}\,\mathrm{cm}^{-3}$, structures are ablated by extremely high intensity of periodic distribution of electrons and holes just around the peaks and troughs of SPP. Structure period approaches to a stable value ranging from 200 nm to 220 nm as shown in Fig. 5(b). If the power is much more above the threshold, period increased a little considering the enhanced SPP reflection. Here, the model is in reasonable agreement with the experimental data such as the induced grating direction and period. Parameters $\varepsilon_{ZnS} = 5.35$ at $\lambda = 800$ nm, $c = 3 \times 10^8$ m/s, $e = 1.6 \times 10^{-19}$ C, $\tau_D = 1$ fs, $m_{opt} = 0.38$, $\varepsilon_0 = 8.8419 \times 10^{-12}$ F/m, and $m_e = 9.11 \times 10^{-31}$ kg were used in the simulation.

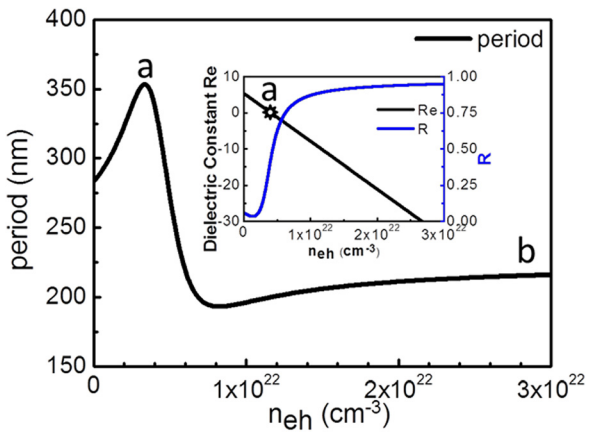

FIG. 5. Structure period with excitation of electrons. The corresponding dielectric constant and reflection of surface was the inset curve.

Another notable phenomenon is the process of laser excited electrons. Energy gap of ZnS is about 3.6 eV which is more than twice of one photon energy 1.55 eV. So it is the three-photon absorption at least in the beginning of excitation process. However, as the formation of SPP, multi-photon will be changed into one-photon absorption.[30] Threshold for the same intensity SPP excitation will be reduced. In other words, their seed structures first formed before the subwavelength structures in shape just as the experiment shown in Fig. 2.

In conclusion, we report here a rapid facile approach to fabricate large area hierarchic structures with femtosecond laser by using a phase mask. The structures are consisted of periodically arranged sub-wavelength nanogratings that could be extended to the area as large as the mask itself only if the incident beam is sufficiently spatially expanded. The nature of the use of the phase mask is light-field tailoring (LFT), and here the role of LFT is provision of periodically distributed wavelets, i.e., its first order diffraction. The wavelets interact with material either by their direct interference or by their interference with induced waves such as SPP or SHG. The transient interference light patterns are then transferred into matter structures by local removal of materials at the sites of light intensity maximum only if the laser pulse energy is properly chosen. The use of a cylindrical lens for rectangular focusing and the laser beam scanning relative to the mask technically ensures the full advantage of the wavelet interference enabled by the phase mask, expanding the dimension of microgratings, and therefore the nanogratings and the entire hybrid structures to desired macroscale. Although not detailed here, the same deep subwavelength structures have been attained in wide-bandgap semiconductors like GaAs, ZnO, and ZnSe, meaning that the technology may find broad application of optoelectronic industry.

The authors gratefully acknowledge the support from 973 Program (Grant No. 2011CB013003 and 2014CB921302) and NSFC (Grant Nos. 61137001, 61127010 and 90923037). In particular, thanks to Professor Michael Withford of Macquarie University for useful discussion.

[1]Y. Shimotsuma, P. G. Kazansky, J. Qiu, and K. Hirao, Phys. Rev. Lett. **91**, 247405 (2003).

[2]R. L. Harzic, H. Schuck, D. Sauer, T. Anhut, I. Riemann, and K. König, Opt. Express **13**, 6651 (2005).
[3]A. Y. Vorobyev, V. S. Makin, and C. Guo, J. Appl. Phys. **101**, 034903 (2007).
[4]J. E. Sipe, J. F. Young, J. S. Preston, and H. M. van Driel, Phys. Rev. B **27**, 1141 (1983).
[5]T. Q. Jia, H. X. Chen, M. Huang, F. L. Zhao, J. R. Qiu, R. X. Li, Z. Z. Xu, X. K. He, J. Zhang, and H. Kuroda, Phys. Rev. B **72**, 125429 (2005).
[6]X. D. Guo, R. X. Li, Y. Hang, Z. Z. Xu, B. K. Yu, H. L. Ma, B. Lu, and X. W. Sun, Mater. Lett. **62**, 1769 (2008).
[7]M. Ivanov and P. Rochon, Appl. Phys. Lett. **84**, 4511 (2004).
[8]W. Xiong, Y. S. Zhou, X. N. He, Y. Gao, M. M.-Samani, L. Jiang, T. Baldacchini, and Y. F. Lu, Light Sci. Appl. **1**, e6 (2012).
[9]S. Juodkazis, V. Mizeikis, and H. Misawa, J. Appl. Phys. **106**, 051101 (2009).
[10]K. Sugioka, Y. Hanada, and K. Midorikawa, Laser Photonics Rev. **4**, 386 (2010).
[11]M. Qian, Y. S. Zhou, Y. Gao, J. B. Park, T. Feng, S. M. Huang, Zh. Sun, L. Jiang, and Y. F. Lu, Carbon **49**, 5117 (2011).
[12]Q.-D. Chen, D. Wu, L.-G. Niu, J. Wang, X.-F. Lin, H. Xia, and H.-B. Sun, Appl. Phys. Lett. **91**, 171105 (2007).
[13]D. Wu, L.-G. Niu, Q.-D. Chen, R. Wang, and H.-B. Sun, Opt. Lett. **33**, 2913 (2008).
[14]M. Born and E. Wolf, *Principles of Optics: Electromagnetic Theory of Propagation, Interference and Diffraction of Light* (Cambridge University Press, London, 1999), Vol. 286.
[15]M. Huang, F. Zhao, Y. Cheng, N. Xu, and Z. Xu, Opt. Express **18**, A600 (2010).
[16]T. Tomita, K. Kinoshita, S. Matsuo, and S. Hashimoto, Appl. Phys. Lett. **90**, 153115 (2007).
[17]T. Tomita, R. Kumai, S. Matsuo, S. Hashimoto, and M. Yamaguchi, Appl. Phys. A **97**, 271 (2009).
[18]L. Wang, B.-B. Xu, Q.-D. Chen, Z.-C. Ma, R. Zhang, Q.-X. Liu, and H.-B. Sun, Opt. Lett. **36**, 3305 (2011).
[19]L. Wang, Z.-H. Lü, X.-F. Lin, Q.-D. Chen, B.-B. Xu, and H.-B. Sun, J. Lightwave Technol. **31**, 276 (2013).
[20]B.-R. Gao, H.-Y. Wang, Y.-W. Hao, L.-M. Fu, H.-H. Fang, Y. Jiang, L. Wang, Q.-D. Chen, H. Xia, L.-Y. Pan, Y.-G. Ma, and H.-B. Sun, J. Phys. Chem. B **114**, 128 (2010).
[21]H. Xia, J. Wang, Y. Tian, Q.-D. Chen, X.-B. Du, Y.-L. Zhang, Y. He, and H.-B. Sun, Adv. Mater. **22**, 3204 (2010).
[22]Y.-L. Zhang, Q.-D. Chen, H. Xia, and H.-B. Sun, Nano Today **5**, 435 (2010).
[23]H.-B. Sun, S. Juodkazis, M. Watanabe, S. Matsuo, H. Misawa, and J. Nishii, J. Phys. Chem. B **104**, 3450 (2000).
[24]G. Miyaji and K. Miyazaki, Opt. Express **16**, 16265 (2008).
[25]J. Bonse, A. Rosenfeld, and J. Krüger, Proc. SPIE **7990**, 79940M (2010).
[26]J.-T. Chen, W.-C. Lai, Y.-J. Kao, Y.-Y. Yang, and J.-K. Sheu, Opt. Express **20**, 5689 (2012).
[27]K. Yoshii, J. K. Anthony, and M. Katsuragawa, Light Sci. Appl. **2**, e58 (2013).
[28]K. Sokolowski-Tinten and D. von der Linde, Phys. Rev. B **61**, 2643 (2000).
[29]M. Straub, M. Afshar, D. Feili, H. Seidel, and K. König, Opt. Lett. **37**, 190 (2012).
[30]R. Taylor, C. Hnatovsky, and E. Simova, Laser Photonics Rev. **2**, 26 (2008).